#### **CONFERENCE PRE-PRINT**

# PROGRESS AND INNOVATIONS IN THE TCV TOKAMAK RESEARCH PROGRAMME

C. THEILER<sup>1</sup>, J. ADAMEK<sup>2</sup>, M. AGOSTINI<sup>3</sup>, C. ALBERT<sup>4</sup>, S. ALBERTI<sup>1</sup>, G. ALBERTI<sup>5</sup>, S. ALEIFERIS<sup>6</sup>, E. ALESSI<sup>7</sup>, G. ANASTASIOU<sup>8</sup>, Y. ANDRÈBE<sup>1</sup>, Y. ANTONENAS<sup>9</sup>, GM. APRUZZESE<sup>10</sup>, L. AUCONE<sup>11</sup>, F.  $AURIEMMA^3$ , J.  $AYLLON^{12}$ , E.  $AYMERICH^{13}$ , F.  $BAGNATO^{14,15}$ , F.  $BAIRAKTARIS^{16}$ , A.  $BALESTRI^1$ , J.  $BALL^1, S.\ BALUGANI^1, M.\ BAQUERO-RUIZ^1, O.\ BARDSLEY^6, A.\ BATTEY^1, T.\ BAUER^{17}, S.\ BECHTLE^{18}, A.\ BATTEY^1, T.\ BAUER^{17}, S.\ BAUER^{17}, S.$ M. BERNERT<sup>19</sup>, W. BIN<sup>7</sup>, P. BLANCHARD<sup>1</sup>, J. BOEDO<sup>20</sup>, T. BOLZONELLA<sup>3</sup>, L. BONALUMI<sup>11</sup>, M. BONISOLLI<sup>1</sup>, T. BOSMAN<sup>21,17</sup>, R. BOUFFET-KLEIN<sup>22</sup>, M.D. BOYER<sup>23</sup>, L. BRAMUCCI<sup>3</sup>, F. BRAUNMÜLLER<sup>1</sup>, D. BRIDA<sup>19</sup>, B. BROWN<sup>1</sup>, S. BRUNNER<sup>1</sup>, J. BUERMANS<sup>24,25</sup>, D. BUSI<sup>5</sup>, Y. CAMENEN<sup>26</sup>, A. CARDINALI<sup>10</sup>, S. CARLI<sup>27</sup>, D. CARNEVALE<sup>28</sup>, F. CARPANESE<sup>1</sup>, M. CARPITA<sup>1</sup>, A. CASOLARI<sup>2</sup>, C. CASTALDO<sup>10</sup>, M. CAVEDON<sup>11</sup>, J. CAZABONNE<sup>1</sup>, J. CEROVSKY<sup>2</sup>, B. CHAPMAN-OPLOPOIOU<sup>6</sup>, O. CHELLAI<sup>1</sup>, Y. CHERVONYI<sup>18</sup>, J. CHLUM<sup>2</sup>, P. CHMIELEWSKI<sup>29</sup>, A. CHOMICZEWSKA<sup>29</sup>, R. CICIONI<sup>3</sup>, G. CIRAOLO<sup>30</sup>, I. CLASSEN<sup>21</sup>, A. CLOD<sup>31</sup>, S. CODA<sup>1</sup>, C. COLANDREA<sup>1</sup>, C. CONTRE<sup>1</sup>, R. COOSEMANS<sup>1</sup>, L. CORDARO<sup>3</sup>, M. CORNELISSEN<sup>17,1</sup>,  $T. CRACIUNESCU^{32}, DJ. CRUZ ZABALA^{12}, M. CZARSKI^{29}, I. DAVIES^{18}, C. DAWSON^{33}, G. DE TOMMASI^{34}, \\$ J. DECKER<sup>1</sup>, G. DERKS<sup>21,17</sup>, E. DEVLAMINCK<sup>1</sup>, G. DI GIANNATALE<sup>1</sup>, LE. DI GRAZIA<sup>34,35</sup>, R. DING<sup>36</sup>, M. DREVAL<sup>37</sup>, C. DRITSELIS<sup>38</sup>, S. DUBBIOSO<sup>34</sup>, R. DUCKER<sup>1</sup>, M. DUNNE<sup>19</sup>, G. DURR-LEGOUPIL-NICOUD<sup>1</sup>, B.P. DUVAL<sup>1</sup>, L. ÉDES<sup>1</sup>, S. ERNST<sup>1</sup>, M. FAITSCH<sup>19</sup>, C. FAN<sup>33</sup>, A. FASOLI<sup>1</sup>, N. FEDORCZAK<sup>30</sup>, F. FELICI<sup>18</sup>, N. FERRON<sup>3</sup>, O. FEVRIER<sup>1</sup>, O. FICKER<sup>2</sup>, L. FIGINI<sup>7</sup>, P. FIGUEIREDO<sup>21</sup>, A. FRANK<sup>1</sup>, L. FRASSINETTI<sup>39</sup>, D. FRATTOLILLO<sup>34</sup>, D. FRIGIONE<sup>3</sup>, I. FURNO<sup>1</sup>, D. GALASSI<sup>1</sup>, G. GALATOLA TEKA<sup>10</sup>, J. GALDON-QUIROGA<sup>12</sup>, S. GALEANI<sup>28</sup>, C. GALPERTI<sup>1</sup>, M. GAMBRIOLI<sup>3</sup>, S. GARAVAGLIA<sup>7</sup>, S. GAR-CIA HERREROS<sup>1</sup>, M. GARCIA MUNOZ<sup>12</sup>, P. GAUDIO<sup>28</sup>, M. GELFUSA<sup>28</sup>, J. GENOUD<sup>1</sup>, S. GERASIMOV<sup>6</sup>, L. GIL<sup>40</sup>, C. GIROUD<sup>6</sup>, P. GIROUD-GARAMPON<sup>1</sup>, M. GOBBIN<sup>3</sup>, T. GOLFINOPOULOS<sup>41</sup>, T.P. GOODMAN<sup>1</sup>, S. GORNO<sup>1</sup>, M. GRANDIN<sup>3</sup>, G. GRANUCCI<sup>15</sup>, F. GRAZIANO<sup>5</sup>, M. GRIENER<sup>19</sup>, N. GRZYBICKA<sup>29</sup>, S.  $GUINCHARD^1, A. \ HAKOLA^{42}, \ P. \ HALLDESTAM^{19}, \ C. \ HAM^6, \ D. \ HAMM^1, \ P. \ HEINRICH^{19}, \ C. \ HEISS^1,$ S. HENDERSON<sup>6</sup>, P. HENNEQUIN<sup>43</sup>, J.-P. HOGGE<sup>1</sup>, R. HOJLUND<sup>31</sup>, C. HONORÉ<sup>43</sup>, M. HOPPE<sup>39</sup>, J.  $HORACEK^2, \ E. \ HUETT^1, \ P. \ INNOCENTE^{44,3}, \ P. \ IVANOV^1, \ V. \ IVANOV^{45}, \ A. \ JANSEN \ VAN \ VUUREN^1,$ A. JARDIN<sup>46</sup>, R. JASPERS<sup>17</sup>, F. JAULMES<sup>2</sup>, T. JENSEN<sup>31</sup>, M. JIMENEZ COMEZ<sup>12</sup>, E. JOFFRIN<sup>30</sup>, D.  $KABIROV^{12}$ , AN.  $KARPUSHOV^1$ , S.  $KASILOV^4$ , Y.  $KAZAKOV^{24}$ , S.  $KERBOUA-BENLARBI^1$ , A.  $KHAN^1$ , D.  $KING^6$ , A.  $KIRJASUO^{42}$ , E.M.M.  $KIVITS^{21}$ , S.  $KOBUSSEN^{21}$ , J.T.W.  $KOENDERS^{21,17}$ , P.  $KOHLI^{18}$ . J. KOLSEN DE WIT<sup>31</sup>, Y. KOMINIS<sup>9</sup>, M. KONG<sup>1</sup>, B. KOOL<sup>21</sup>, J. KOVACIC<sup>47,48</sup>, D. KROPACKOVA<sup>45</sup>, O. KRUTKIN<sup>1</sup>, U. KUMAR<sup>1</sup>, R. KWIATKOWSKI<sup>49</sup>, M. LA MATINA<sup>3</sup>, B. LABIT<sup>1</sup>, A. LAFAY<sup>39</sup>, V. LAPORTA<sup>50</sup>, K. LEE<sup>1</sup>, F. LENGYEL<sup>51,52</sup>, K. LIM<sup>1</sup>, B. LINEHAN<sup>41</sup>, A. LISTOPAD<sup>1</sup>, L. LOBKO<sup>45</sup>, N. LONIGRO<sup>6</sup>, T. LUNT<sup>19</sup>, R. MACKENBACH<sup>1</sup>, E. MACUSOVA<sup>2</sup>, P. MAGET<sup>30</sup>, S. MALEC<sup>45</sup>, D. MANCINI<sup>1</sup>, P. MANTICA<sup>7</sup>, C. MARCHETTO<sup>53</sup>, S. MARCHIONI<sup>1</sup>, A. MARIANI<sup>7</sup>, M. MARIN<sup>1</sup>, A. MARINONI<sup>41,20</sup>, M. MARKL<sup>4</sup>, Y. MARTIN<sup>1</sup>, L. MARTINELLI<sup>1</sup>, S. MASILLO<sup>1</sup>, R. MASOCCO<sup>28</sup>, V. MASSON<sup>1</sup>, M. MATTEI<sup>34</sup>, S. MATTOGNO<sup>28</sup>, D. MAZON<sup>30</sup>, S. MAZZI<sup>30</sup>, A. MELE<sup>1</sup>, V. MENKOVSKI<sup>17</sup>, A. MERLE<sup>1</sup>, A. MICHI<sup>18</sup>, R. MIROWSKI<sup>49</sup>, S. MISDANITIS<sup>38</sup>, R. MISHRA<sup>29</sup>, D. MOIRAF<sup>30</sup>, P.A. MOLINA-CABRERA<sup>1</sup>, S. MOLISANI<sup>3</sup>, F. MOMBELLI<sup>5</sup>, R. MORGAN<sup>1</sup>, A. MORO<sup>7</sup>, A. MURARI<sup>3,44</sup>, K. MURRAY<sup>6</sup>, P. MUSCENTE<sup>41</sup>, I. MUZIO<sup>1</sup>, D. MYKYTCHUK<sup>1</sup>, Y. NAKEVA<sup>54</sup>, F. NAPOLI<sup>10</sup>, A. NIELSEN<sup>31</sup>, SK. NIELSEN<sup>31</sup>, T. NORMAN<sup>18</sup>, S. NOWAK<sup>7</sup>, H. NYSTRÖM<sup>39</sup>, R. OCHOUKOV<sup>19</sup>, A. ORDUNA MARTINEZ<sup>19</sup>, L. ORLANDI<sup>3</sup>, C. ORRICO<sup>17</sup>, FP. ORSITTO<sup>34</sup>, R. OSAWA<sup>6</sup>, N. OSBORNE<sup>6,55</sup>, P. OYOLA<sup>12</sup>, A. PAJARES<sup>56</sup>, DI. PALADE<sup>32</sup>, O. PAN<sup>19</sup>, O. PANICO<sup>1</sup>, P. PAPAGIANNIS<sup>16</sup>, M. PASSONI<sup>5</sup>, F. PASTORE<sup>1</sup>, AH. PATEL<sup>19</sup>, A. PAU<sup>1</sup>, C. PAZ-SOLDAN<sup>57</sup>, A.C. PEDERSEN<sup>31</sup>, M. PEDRINI<sup>1</sup>, G. PELKA<sup>29</sup>, A. PEREK<sup>1</sup>, Y. PERES ASNIS<sup>1</sup>, R. PERILLO<sup>20</sup>, F. PESAMOSCA<sup>14</sup>, K. PETERSEN<sup>31</sup>, L. PIGATTO<sup>3</sup>, C. PIRON<sup>3,58</sup>, L. PIRON<sup>3</sup>, A. PIRONTI<sup>34</sup>, V. PLYUSNIN<sup>40</sup>, M. PODESTA<sup>1</sup>, Y. POELS<sup>1</sup>, G.  $POKOL^{51}, J.\ POLEY^{1}, L.\ POM\^{R}JANSCHI^{32}, M.\ PORADZINSKI^{29}, L.\ PORTE^{1}, C.\ POSSIERI^{28}, F.\ PUENTES$ DEL POZO<sup>12</sup>, M.J. PUESCHEL<sup>21,17</sup>, V. QUADRI<sup>30</sup>, M. RABINSKI<sup>49</sup>, R. RAGONA<sup>31</sup>, G. RATTA<sup>59</sup>, C. REA<sup>41</sup>, H. REIMERDES<sup>1</sup>, M. REISNER<sup>19</sup>, C. REUX<sup>30</sup>, D. RICCI<sup>7</sup>, P. RICCI<sup>1</sup>, S. RIENACKER<sup>43</sup>, N. RISPOLI<sup>7</sup>, JF.  $RIVERO-RODRIGUEZ^{12,6}, R.\ RIZKALLAH^{20}, A.\ RODRIGUEZ\ GONZALEZ^{12}, F.\ ROMANO^1, R.\ ROSSI^{28}, A.\ RODRIGUEZ^{12,6}, R.\ RIZKALLAH^{20}, R.\ RIZ$  $M.\ RUD^{31,1},\ D.\ SALES\ DE\ OLIVEIRA^1,\ M.\ SALEWSKI^{31},\ A.\ SALMI^{42},\ O.\ SAUTER^1,\ BO\ S\ SCHMIDT^{31},$ N. SCHOONHEERE<sup>30</sup>, K. SCHUTJES<sup>17</sup>, L. SCOTTI<sup>11</sup>, L. SENNI<sup>10</sup>, M.G. SENSTIUS<sup>60</sup>, S. SETZU<sup>13</sup>, S. SHARAPOV<sup>6</sup>, U.A. SHEIKH<sup>1</sup>, G. SIAS<sup>13</sup>, M. SILVA FÜGLISTER<sup>1</sup>, D. SILVAGNI<sup>19</sup>, A. SIMONETTO<sup>7</sup>, L.

SIMONS<sup>1</sup>, L. SINGH<sup>30</sup>, K. SINGH<sup>1</sup>, P. SINTRE<sup>1</sup>, S. SIPILÄ<sup>61</sup>, O. SO<sup>33</sup>, C. SOMMARIVA<sup>1</sup>, C. SOZZI<sup>7</sup>, S. SPAGNOLO<sup>3</sup>, A. STAGNI<sup>3,58</sup>, C. STOLLBERG<sup>1</sup>, F. SUBBA<sup>62</sup>, G. SUN<sup>1</sup>, H. SUN<sup>1</sup>, J. SVANTNER<sup>1</sup>, T. TALA<sup>42</sup>, P. TAMAIN<sup>30</sup>, K. TANAKA<sup>63</sup>, W. TANG<sup>19</sup>, A. TEMA BIWOLE<sup>1</sup>, A. TENAGLIA<sup>28</sup>, D. TERRANOVA<sup>3,44</sup>, D. TESTA<sup>1</sup>, K. THOME<sup>56</sup>, A. THRYSOE<sup>31</sup>, M. TOMES<sup>2</sup>, E. TONELLO<sup>1</sup>, B. TRACEY<sup>18</sup>, E. TSITRONE<sup>30</sup>, C.K. TSUI<sup>20,56</sup>, J. TUMBOKON<sup>1</sup>, M. TUNKL<sup>45</sup>, M. UGOLETTI<sup>3</sup>, A. VALENTINI<sup>31</sup>, M. VALLAR<sup>1</sup>, M. VAN BERKEL<sup>21</sup>, L. VAN LEEUWEN<sup>17,21</sup>, S. VAN MULDERS<sup>14,1</sup>, G. VAN PARYS<sup>1</sup>, M. VAN ROSSEM<sup>1</sup>, C. VENTURINI<sup>1</sup>, K. VERHAEGH<sup>17</sup>, L. VERMARE<sup>43</sup>, N. VIANELLO<sup>3,44</sup>, E. VIEZZER<sup>12</sup>, L. VILLARD<sup>1</sup>, B. VINCENT<sup>1</sup>, C. VINCENT<sup>6</sup>, P. VINCENZI<sup>3</sup>, J. VINKLÁREK<sup>45</sup>, I. VOITSEKHOVITCH<sup>6</sup>, L. VOTTA<sup>39</sup>, N.M.T. VU<sup>14</sup>, A. WANG<sup>41,33</sup>, C. WANG<sup>1</sup>, Y. WANG<sup>1</sup>, N. WENDLER<sup>29</sup>, E. WESTERHOF<sup>21</sup>, S. WIESEN<sup>21</sup>, T. WIJKAMP<sup>17</sup>, M. WINKEL<sup>17</sup>, C. WÜTHRICH<sup>1</sup>, I. WYSS<sup>28</sup>, L. XIANG<sup>6</sup>, G. XU<sup>36</sup>, H. YANG<sup>30</sup>, J. ZEBROWSKI<sup>49</sup>, M. ZERBINI<sup>10</sup>, P. ZESTANAKIS<sup>8</sup>, H. ZHANG<sup>1</sup>, B. ZIMMERMANN<sup>19</sup>, M. ZUIN<sup>3,44</sup>, M. ZURITA<sup>1</sup>

- <sup>1</sup> École Polytechnique Fédérale de Lausanne (EPFL), Swiss Plasma Center (SPC), Lausanne, Switzerland
- <sup>2</sup> Institute of Plasma Physics of the CAS, Prague, Czech Republic
- <sup>3</sup> Consorzio RFX, Padova, Italy
- <sup>4</sup> Institut für Theoretische Physik, Technische Universität Graz, Graz, Austria
- <sup>5</sup> Politecnico di Milano, Milan, Italy
- <sup>6</sup> United Kingdom Atomic Energy Authority, Culham Science Centre, Abingdon, Oxfordshire, UK
- <sup>7</sup> Istituto per la Scienza e Tecnologia dei Plasmi ISTP-CNR, Milano, Italy
- <sup>8</sup> Aristotle University of Thessaloniki, Thessaloniki, Greece
- <sup>9</sup> School of Applied Mathematical and Physical Sciences, National Technical University of Athens, Athens, Greece
- <sup>10</sup> Unità Tecnica Fusione, ENEA, Frascati, Italy
- <sup>11</sup> Università di Milano-Bicocca, Milano, Italy
- <sup>12</sup> Universidad de Sevilla, Sevilla, Spain
- <sup>13</sup> Dept. of Electrical and Electronic Engineering, University of Cagliari, Cagliari, Italy
- <sup>14</sup> ITER Organization, Saint-Paul-lez-Durance, France
- <sup>15</sup> DTT S.C.a.r.l., Frascati, Italy
- <sup>16</sup> Department of Physics, National and Kapodistrian University of Athens, Athens, Greece
- <sup>17</sup> Eindhoven University of Technology, Eindhoven, Netherlands
- <sup>18</sup> Google DeepMind, London, UK
- <sup>19</sup> Max Planck Institute for Plasma Physics, Garching, Germany
- <sup>20</sup> Center for Energy Research (CER), University of California-San Diego (UCSD), La Jolla, CA, USA
- <sup>21</sup> DIFFER-Dutch Institute for Fundamental Energy Research, Eindhoven, Netherlands
- <sup>22</sup> ENS Paris-Saclay, Gif-sur-Yvette, France
- <sup>23</sup> Commonwealth Fusion Systems (CFS), Devens, MA, USA
- <sup>24</sup> Laboratory for Plasma Physics, LPP-ERM/KMS, Brussels, Belgium
- <sup>25</sup> Department of Applied Physics, Ghent University, Ghent, Belgium
- <sup>26</sup> Aix-Marseille Université, CNRS, Marseille, France
- <sup>27</sup> Department of Mechanical Engineering, KU Leuven, Leuven, Belgium
- <sup>28</sup> University of Rome Tor Vergata, Rome, Italy
- <sup>29</sup> Institute of Plasma Physics and Laser Microfusion (IPPLM), Warsaw, Poland
- <sup>30</sup> CEA, IRFM, Saint Paul-Lez-Durance Cedex, France
- <sup>31</sup> Department of Physics, Technical University of Denmark, Kgs, Lyngby, Denmark
- <sup>32</sup> National Institute for Laser, Plasma and Radiation Physics, Bucharest-Magurele, Romania
- <sup>33</sup> Laboratory for Information and Decision Systems (LIDS), Massachusetts Institute of Technology, Cambridge, MA, USA
- <sup>34</sup> Università degli Studi di Napoli 'Federico II', Consorzio CREATE, Napoli, Italy
- <sup>35</sup> Università degli Studi della Campania 'L. Vanvitelli', Aversa, Italy
- 36 Institute of Plasma Physics, Hefei Institutes of Physical Science, Chinese Academy of Sciences, Hefei, China
- <sup>37</sup> Institute of Plasma Physics of the NSC KIPT, Kharkov, Ukraine
- <sup>38</sup> Department of Mechanical Engineering, University of Thessaly, Volos, Greece
- <sup>39</sup> KTH Royal Institute of Technology, Stockholm, Sweden
- <sup>40</sup> Instituto de Plasmas e Fusã o Nuclear, Instituto Superior Técnico, Lisboa, Portugal
- <sup>41</sup> Plasma Science and Fusion Center (PSFC), Massachusetts Institute of Technology, Cambridge, MA, USA
- <sup>42</sup> VTT Technical Research Centre of Finland, Espoo, Finland
- <sup>43</sup> Laboratoire de Physique des Plasmas (LPP), CNRS, Sorbonne Université, École polytechnique, Institut Polytechnique de Paris, Palaiseau, France
- <sup>44</sup> Istituto per la Scienza e Tecnologia dei Plasmi ISTP-CNR, Padova, Italy
- <sup>45</sup> Faculty of Nuclear Sciences and Physical Engineering, Czech Technical University in Prague, Prague, Czech Republic
- <sup>46</sup> Institute of Nuclear Physics Polish Academy of Sciences (IFJ PAN), Krakow, Poland
- <sup>47</sup> Jožef Stefan Institute, Ljubljana, Slovenia
- <sup>48</sup> University of Ljubljana, Lyubljana, Slovenia
- <sup>49</sup> National Centre for Nuclear Research (NCBJ), Otwock, Poland
- <sup>50</sup> Istituto per la Scienza e Tecnologia dei Plasmi, Bari, Italy

- <sup>51</sup> Centre for Energy Research, Budapest, Hungary
- <sup>52</sup> Budapest University of Technology and Economics, Budapest, Hungary
- <sup>53</sup> CNR & Dip. di Energia, Politecnico di Torino, Turin, Italy
- <sup>54</sup> Department of Economics, Engineering, Society and Business Organization (DEIm), University of Tuscia, Viterbo, Italy
- <sup>55</sup> University of Liverpool, Liverpool, UK
- <sup>56</sup> General Atomics, San Diego, CA, USA
- <sup>57</sup> Columbia University, New York, NY, USA
- <sup>58</sup> Università degli Studi di Padova, Padova, Italy
- <sup>59</sup> Laboratorio Nacional de Fusión, CIEMAT, Madrid, Spain
- 60 Rudolf Peierls Centre for Theoretical Physics, University of Oxford, Oxford, UK
- <sup>61</sup> Aalto University, Aalto, Finland
- 62 NEMO Group, Politecnico di Torino, Torino, Italy
- 63 National Institute for Fusion Science, Toki, Gifu, Japan

Email: christian.theiler@epfl.ch

# **Abstract**

Research on TCV addresses a wide range of key questions relevant to ITER and future fusion power plants. Over the past two years, highly productive experimental campaigns have led to major advances across several areas: the ITER baseline scenario; pedestal properties in low-collisionality, peeling-limited conditions; and the development of high- $\beta_N$ , non-inductive regimes. Alternative high-power scenarios have likewise received significant attention, with remarkable progress in quasicontinuous exhaust operation, X-point radiator plasmas, and negative triangularity configurations. Substantial achievements were also made in the mitigation or benign termination of runaway electron beams, in elucidating fast-ion loss mechanisms, and in improving exhaust behavior in both conventional and alternative divertor geometries. These experimental results have been strongly supported by advances in modelling and their direct application to the experiment, ranging from gyrokinetic simulations of core and pedestal turbulence to fluid-based studies of scrape-off layer and divertor physics in diverse geometries. Plasma control has taken on an increasingly important role, with model-based and data-driven approaches now closely intertwined with physics studies. This preprint provides a overview of these recent activities, together with an outlook on forthcoming upgrades and next steps, while a more comprehensive review will appear in the accompanying Nuclear Fusion journal article.

## 1. INTRODUCTION

The Tokamak à Configuration Variable (TCV, major radius  $R\approx 0.88\mathrm{m}$ , aspect ratio  $A\approx 3.5$ , toroidal field  $B\leq 1.5\mathrm{T}$ ) is a highly flexible and versatile research facility operated at the Swiss Plasma Center of the Swiss Federal Institute of Technology Lausanne (EPFL) [1, 2]. It features unique magnetic shaping capabilities, excellent diagnostics, a modern control system, and versatile heating systems - currently consisting of 2.6 MW Neural Beam Injection (NBI) and a total of 3.6 MW of second (X2) and third (X3) harmonic Electron Resonance Cyclotron Heating (ECRH) power. Two additional, 1MW, dual-frequency gyrotrons are foreseen for 2026. Operated partly as a European facility within the EUROfusion Tokamak Exploitation Work Package (WPTE)[3], research on TCV tackles key challenges for ITER and fusion power plants while contributing strongly to the education of young researchers.

Following a complete overhaul of neutron and gamma-ray shielding in early 2023, TCV now operates without radiation-imposed limits despite recent increases in neutral beam injection power capabilities [4]. The fourth major refurbishment of TCV's flywheel generator made it ready for the next ten years of operation [5] and improvements in the preparation and data-quality monitoring of the standard TCV diagnostics improved experimental efficiency [6]. The 2023-2025 campaigns were highly productive, featuring four different divertor closures and attaining a record of 3'517 successful plasma discharges in 2024, while simultaneously preparing for various upgrades.

This paper presents an overview of the research activities and the progress achieved on TCV over the past two years, since the last IAEA-FEC conference in London in October 2023.

# 2. PLASMA SCENARIOS - H-MODE AND ALTERNATIVE ELM-FREE REGIMES

TCV has focused significant efforts on the study and preparation for operating the 'standard' inductive ELMy H-mode scenario foreseen for ITER, the ITER Base-Line (IBL). NBI and ECRH heated IBL scenarios were developed and analysed [7], using the strategy to enter H-mode at large  $q_{95}$  and reduced shaping. Three different ITER shapes were reproduced, the JET IBL, the AUG IBL, and the ITER IBL. The experiments displayed increasing ELM perturbations and enhanced difficulty to reach stationary conditions for increasing top triangularity. Good performance ( $H_{98} \sim 1.2, \beta_N \sim 1.6$ ) was demonstrated for several energy confinement times, usually followed

by the onset of neoclassical tearing modes (NTMs). Avoidance of this NTM onset with X3 heating succeeded at medium  $\beta_N$  and high  $q_{95}$ , but was constrained at ITER  $q_{95}$  due to density peaking and weak X3 absorption. Integrated modelling using ASTRA-GLF23 quasi-linear drift model-based transport identified ITGs as the dominant core instability in these plasmas and reproduced the turbulent-driven density peaking. More recent scenarios with up to 90% X3 absorption featured large, regular ELMs and avoided NTMs but at lower  $q_{95}$  than the IBL.

A parameter that cannot be matched in IBL studies on today's devices is the pedestal collisionality. As part of a EUROfusion multi-device effort that also includes JET and MAST-U, significant work has been dedicated to extending TCV's pedestal studies towards ITER-relevant, low- $\nu^*$ , peeling-limited conditions [8]. This was achieved by operating at low density and high power with both NBI and ECRH, reaching low-n peeling-mode-unstable pedestals with Type-I ELMs. D<sub>2</sub> fuelling scans showed that, unlike in ballooning-limited pedestals, the pedestal pressure increases with  $n_{e,ped}$ , a behaviour ascribed to the stabilising effect of density on peeling modes. Consistently with JET and MAST-U, the TCV results furthermore showed that the pedestal pressure does not degrade with increasing  $n_{e,sep}/n_{e,ped}$  in these low- $\nu^*$  conditions, Fig. 1. These results are consistent with Europed, and preliminary extrapolations suggest that this favorable behaviour extends to ITER conditions. Extension of these studies from deuterium to hydrogen plasmas showed qualitatively similar results. In contrast, the pedestal pressure was found to degrade with  $N_2$  seeding, for reasons that are not yet understood [8].

A key aspect in view of ITER operation is an improved understanding of the power threshold for accessing H-mode,  $P_{LH}$ , and its various dependencies. To this end, systematic  $P_{LH}$  studies previously carried out on TCV in Ohmic plasmas via  $I_p$  ramps have been extended to predominantly NBI-heated plasmas [9]. With the plasma shape held fixed, a broad parameter space was explored by scanning the core density,  $I_p$ , and the main ion species (H, D, He) as well as their mixtures. For deuterium plasmas at  $q_{95} \approx 3.3$ , the observed scaling aligns well with the ITPA scaling law. The most notable result was that, across all densities,  $P_{LH}$  increased as  $I_p$  was reduced, consistent with the interpretation that improved L-mode confinement facilitates the L-H transition.

Following TCV's extensive history of steady-state, fully noninductive operation using X2 Electron Cyclotron Current Drive (ECCD), and in preparation for long-pulse scenarios on JT-60SA and ITER, significant recent progress has been made in experimentally developing advanced scenarios with more balanced  $T_e$  and  $T_i$ [10]. Guided by ASTRA modeling, various heating and current drive configurations were established, combining the three existing X2 gyrotrons - each with independent launchers - and the two NBIs. A narrow operational range in density, constrained by the ECRH-X2 cutoff and NBI coupling efficiency, required good density control and specific timing of the heating sources. Non-inductive internal transport barrier (ITB) scenarios transiently achieved record core  $T_e$  values of 12 keV and  $\beta_N \approx 1.85$ , but were restricted to the ECRH-only phase and to  $T_e \gg T_i$ . The addition of NBI heating led to a progressive degradation in performance. A more promising route proved to be approaches with more balanced NBI-1, NBI-2, and ECRH, evolving into a fully non-inductive semi-stationary scenario with  $\beta_N \approx 2$ .

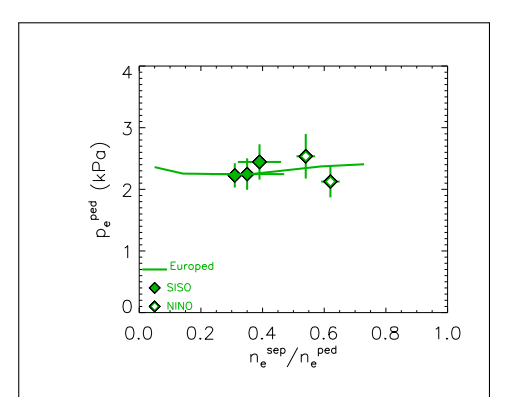


FIG. 1. Measured and simulated pedestal pressure at low  $\nu^{\star}$ , showing no degradation with increasing  $n_{e,sep}/n_{e,ped}$  [8].

Although gradients in density and temperature increased locally at mid-radius and near the edge, a strong ITB or edge transport barriers (ETB) were not observed. As a result, the bootstrap current fraction remained modest ( $\sim 30\%$ ). A promising strategy to address this limitation involves the forthcoming fourth X2 gyrotron, which will enable more central heating. This will complement the existing gyrotrons used in off-axis co-ECCD, enhancing sustainment of the scenario. With these advancements, there is now a realistic prospect of achieving a fully stationary, high- $\beta_N$ , non-inductive, NBI-heated scenario.

Alternative, high-confinement scenarios without large Type-I ELMs continued to be a strong focus on TCV [11]. One promising candidate is the quasi-continuous exhaust (QCE) regime, a well-established operational mode achieved at high shaping and high fuelling. Its access is attributed to unstable ballooning modes localised near the separatrix, which prevent the pedestal from reaching the global peeling-ballooning limit and thus suppress the onset of Type-I ELMs. Consistent with this interpretation, a multi-diagnostic turbulence study identified a weakly coherent mode just inside the separatrix, at  $f \approx 50$  kHz and  $k_{\theta} \approx 100 \text{m}^{-1}$ [12]. Progress in understanding the QCE regime, supported by a step-ladder approach involving TCV and AUG, has led to the successful development of the QCE in JET [11]. Experiments on the three devices revealed a trend of decreasing collisionality for QCE operation with increasing machine size, which, together with predictive modelling, points to QCE as a potential default operational regime for ITER and DEMO. The SOL properties in the QCE regime have been investigated in

high-density H-mode plasmas by increasing the upper triangularity from 0.0 to 0.6, resulting in a transition from Type-I ELMy H-mode to QCE [13]. Both the SOL fall-off lengths of power ( $\lambda_q$ ) and density ( $\lambda_n$ ) increased by a factor of 2.5 across this scan, correlating with the turbulence control parameter  $\alpha_t$  and suggesting a transition to resistive ballooning-dominated SOL turbulence under high-density H-mode conditions. The QCE regime was further associated with the formation of a density shoulder, correlated with an increased filament frequency at the first wall.

The X-Point Radiator (XPR) is another attractive alternative H-mode regime. It offers high radiated power fraction and often achieves full detachment and full ELM suppression, though at the cost of a potential increase in core impurity concentrations and confinement degradation [14]. The existence of an XPR in LSN, seeded H-mode on TCV has been demonstrated both experimentally and through SOLPS-ITER simulations [15]. Its operating window, however, was found to be narrow, as predicted by analytical models for C-wall machines. This window was dramatically broadened by modifying the magnetic geometry [16]. Positioning a secondary X-point near the separatrix, at some distance from the primary X-point in a snowflake-minus shape, enabled the transition to a stable, fully ELM-suppressed XPR without impurity seeding. Confinement and pedestal parameters remained comparable to the preceding Type-I ELMy phase, while  $Z_{eff}$  increased by approximately 50%. This snowflakeminus geometry features a long connection length from the outboard midplane to just above the primary X-point, an extended interface with the high neutral density reservoir in the private flux region, and large poloidal flux expansion in the X-point region toward the core - all features that are theoretically expected to facilitate XPR access. In contrast, configurations closer to an ideal snowflake, sharing only some of these features, did not enable access to the regime. Interestingly, these experiments also showed that an XPR with ELM suppression is not synonymous with divertor detachment. Overall, this work provides an excellent testbed for further XPR model validation.

Negative triangularity (NT) core plasmas, pioneered on TCV, offer a promising route to achieving high-confinement operation while remaining in L-mode, thereby avoiding ELMs and the constraint of operating above the L–H threshold. Significant recent progress has been achieved in the development of NT scenarios with high input power and high core-performance using NBI [17]. These scenarios reach stationary conditions with  $\beta_N \sim 1.8$  and  $H_{98} \sim 1$ , close to those in positive triangularity (PT) H-mode operation on TCV. They are compatible with the TCV baffles and feature higher central ion and electron temperatures than equivalent PT L- and H-mode scenarios. Substantial progress was achieved in divertor detachment and core-edge integration of these and other NT scenarios, and in the theoretical understanding and extrapolation capabilities of NT physics, as detailed in the following.

Ohmic L-mode detachment of the outer divertor via core density ramps was investigated across a wide range of upper, lower, and average triangularity, universally finding detachment more difficult to achieve in NT [18]. While partly explained by differences in divertor geometry, as supported by SOLPS-ITER simulations applying the same transport coefficients in NT and PT [19], significant differences persisted in geometries with fixed divertor geometry, where only the upper triangularity was varied. Increasing the neutral pressure in NT using TCV's divertor baffles, approaching the levels in unbaffled PT plasmas, reduced the outer target temperature. However, detachment remained more difficult to achieve than in PT [20]. These results could at least partly be explained by a narrower  $\lambda_q$  in NT than in PT L-mode, an effect understood theoretically [21] and confirmed experimentally [22]. Simulations with SOLPS-ITER [23] and SOLEDGE2D-EIRENE [24] suggested that a reduction in particle rather than heat diffusivity in NT is needed to match the experimental findings. Despite these challenges, in the baffled, high-performance NT NBI scenarios, outer divertor detachment with an X-point radiator was achieved through nitrogen seeding [17]. Combining this core scenario with a snowflake divertor further allowed for a substantial cooling of the inner strikepoint as well [25]. As in PT H-mode, core performance degraded with seeding, but could be recovered through real-time adjustments of NBI power, overall highlighting NT's potential for core-edge integration.

Theoretical studies and gyrokinetic simulations of core turbulence and transport in NT - motivated by and partly validated on TCV - have improved our understanding and extrapolation capabilities. In Ion Temperature Gradient (ITG) dominated plasmas simulated with GENE, NT was predicted to be more stable than PT for any value of aspect ratio A and for any plasma elongation  $\kappa > 1$  [26, 27]. For Trapped Electron Mode (TEM) dominated turbulence, instead, the benefits of NT were found to be limited to large and conventional A. Global ORB5 simulations in the electrostatic limit predicted no size scaling in the NT transport reduction, suggesting that the favorable transport properties of NT could extrapolate well to reactor conditions [28]. At reactor-relevant, high  $\beta_N$ , electromagnetic instabilities like Micro-Tearing Modes (MTMs) tend to dominate and these modes were found to be more unstable in NT than in PT. However, due to the low magnetic shear in DEMO-scale devices, simulations predicted ITG-dominated turbulence, where NT remained highly favorable [27]. TCV experiments and numerical investigations of PT and NT plasmas in the shapes foreseen for DTT showed promising results, despite DTT's limited NT shaping capabilities, supporting future NT studies at larger size and field than possible today [29, 30].

#### 3. RUNAWAY-ELECTRON PREVENTION AND MITIGATION

Runaway Electron (RE) beams constitute a major threat for a reactor, from discharge startup to termination. Recent TCV experiments [31] demonstrated that central ECRH heating induces enhanced transport, which in turn reduced existing RE seed populations by up to three orders of magnitude. Furthermore, the reduced loop voltage decreased seed generation. In a reactor context, such seed expulsion could expel startup REs and avoid post-disruption RE formation or avert a transition to the dangerous slideaway regime, motivating further studies for extrapolation to reactor-size devices. Complementary to seed expulsion, RE dynamics could also be influenced by momentum-space effects. The resonant interaction between the RE gyromotion and the toroidal magnetic field ripple was shown to explain the anomalously high RE pitch angles in TCV, providing direct experimental evidence of RE momentum-space engineering [32]. This effect resulted in enhanced synchrotron radiation power loss, limiting RE energy.

Once a post-disruption RE beam has formed, the focus shifts to its termination. Benign Termination (BT), relying on large MHD instabilities to expel REs over a broad wetted area while converting magnetic energy into radiation, has emerged as a promising strategy [33]. BT requires the background companion plasma to have low electron density, achieved in a specific neutral pressure range, which enables the fast growing MHD instability required, Fig. 2. The lower limit of this range was studied, for the first time, with SOLPS-ITER, reproducing experimental trends and highlighting the importance of power dissipation via neutral energy conduction to the walls [34]. The upper neutral pressure limit for BT was explored with a particle balance model and through comparisons with experiments [35], indicating that RE impact ionization plays a significant role in increasing the companion plasma density.

Runaway electron (RE) studies on TCV have benefited, and continue to improve, from diagnostic improvements. A new gamma-ray detector, LaBrDoRE (Lanthanum Bromide Detector of Runaway Electrons), was developed [36], which allows monitoring the RE population by measuring the Bremsstrahlung emission in the 1-30 MeV range, generated when REs interact with plasma-facing components. TCV's unique Fast Ion Loss Detector (FILD) allowed, for the first time in magnetically confined plasmas, to obtain direct velocity-space resolved measurements of RE losses [37]. Velocity space mapping with this novel approach revealed both countercurrent (passing) and co-current (trapped and passing) REs with energies in the range 3 MeV < E < 6 MeV and pitch values  $\lambda$  =  $v_{\parallel}/v$  of -0.90 <  $\lambda$  < -0.75 and 0.55 <  $^{"}\lambda$  < 0.80, respectively. Spectrograms of the FILD signal and their correlation with fast magnetic measurements further point to interaction and transport of REs with low-frequency plasma instabilities.

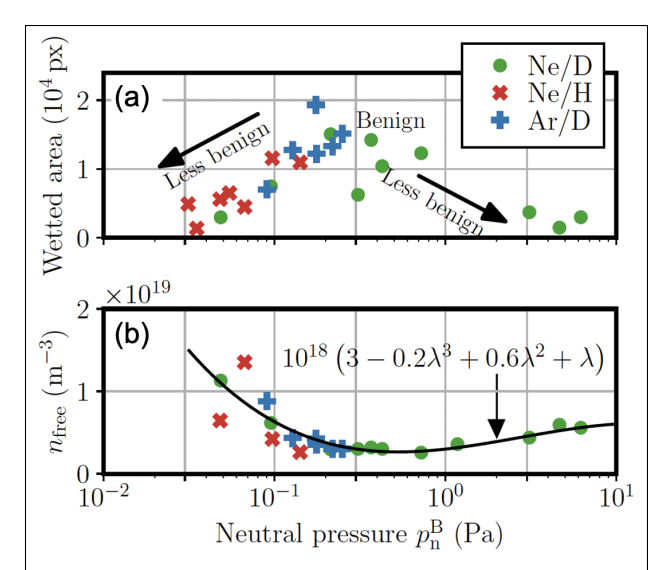


FIG. 2. Neutral pressure dependence of (a) wetted area and (b) density of the background companion plasma during RE experiments. Benign RE beam termination corresponds to large wetted areas, achieved at intermediate neutral pressures. Figure from [35].

# 4. ALFVÉN EIGENMODES AND FAST ION PHYSICS

Alfvén Eigenmode (AE) and Fast Ion (FI) studies have greatly advanced on TCV, supported by improvements in NBI [4] and diagnostic capabilities [38, 39, 40]. Scenarios with unstable AEs were developed in counter NBI plasmas, showing an increase in  $T_i$  and no degradation of confinement time despite increasing NBI power, possibly related to AE-triggered zonal flows [41]. Flux-tube gyrokinetic simulations highlighted the need for a global approach on TCV due to the coupling of AEs and TEM turbulence and the development of radially elongated streamers. NBI-generated FIs were also shown to destabilise energetic particle driven geodesic acoustic modes (EGAMs) at sufficiently high fast particle pressure and low q, and the EGAM's detailed structure and non-rotating character was identified using multichannel SXR and AXUV diagnostics [42].

Systematic studies on the efficiency of ECRH and ECCD to stabilise AEs and the FI losses associated with AEs

received particular attention [43]. On-axis ECRH demonstrated robust stabilisation of counter-NBI driven AEs when the ECRH deposition overlapped the mode location, albeit requiring significant input power ( $\sim 1.5 MW$  of gyrotron power). On-axis counter-current ECCD also enabled effective AE suppression, while co-current drive showed AE mitigation. Suppression and mitigation mechanisms involved not only shear profile modifications, but also significant changes in plasma density and temperature, with the respective roles of these mechanisms yet to be quantified.

FI loss dynamics have been studied extensively, due to their risk of reducing heating efficiency and damaging plasma-facing components in future reactors. As a key diagnostic to probe FI losses, a unique FILD system has been designed, manufactured, and commissioned on TCV [38, 39]. It allows simultaneously measuring the co- and counter-current FI losses in forward and reverse magnetic field and is sensitive to both positively and negatively (see Sec. 3) charged particles across the complete range of operational conditions. It features a two-camera system: a CMOS camera offering high-spatial resolution with medium-temporal resolution and a APD array providing medium-spatial resolution (sufficient for velocity space mapping) with high, MHz temporal resolution. Combined with a new version of the FILDSIM code [40], this system enables high-quality velocity-space sensitive FI reconstructions.

FI loss studies in low-collisionality peeling-limited [45] and high-collisionality IBL-like [44] scenarios revealed distinct inter- and intra-ELM FI transport. Significant inter-ELM FI losses were identified and linked to AEs and NTMs, respectively, in these regimes. The first-time, microsecond, velocity-space (energy E and pitch  $\lambda$ ) resolved FI loss measurements allowed to recover the filamentary and burst-like velocity-space dynamics of the FI losses, exhibiting different pitch and energy values before, during and after the ELM onset. In the IBL-like scenario, magnetic fluctuations of a m/n=2/1 NTM at  $\sim$ 25 kHz and its harmonics were clearly visible also in the FILD signal, highlighting the associated FI losses. Instead, the higher-frequency magnetic fluctuations did not significantly contribute to the FILD signal and thus the FI losses. During the ELM, the FILD signal was characterised by a broadband spectrum, with the 25 kHz mode still present. The pitch-space mapped signal of a single ELM, Fig.

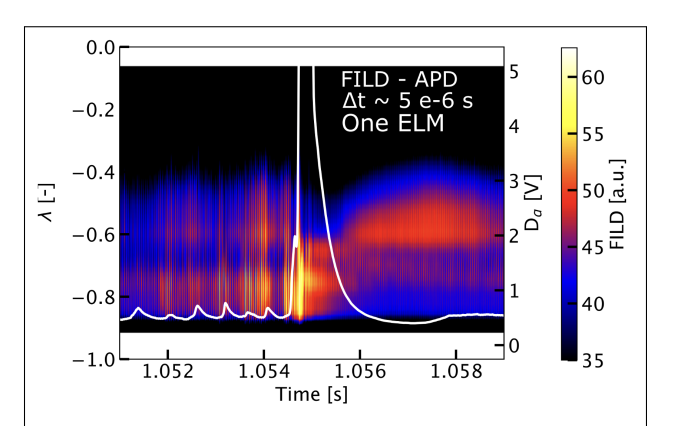


FIG. 3. First-time, microsecond, velocity-space resolved FI loss measurement, here for the FI pitch, during a single ELM. The ELM  $D_{\alpha}$  trace is overlayed in white. Figure from [44].

3, revealed strong loss levels in the vicinity of  $\lambda$  = -0.6 and -0.8. According to ASCOT5 orbit-following simulations, the losses at  $\lambda$  = -0.6 are associated with neoclassical losses while the losses at  $\lambda$  = -0.8 are associated with anomalous transport linked to the low-frequency MHD activity, and peaked during the ELM crash. Both high-collisionality IBL and low-collisionality peeling-limited scenarios showed significant FI acceleration during the ELM crash [45, 44], resulting in FI energies exceeding the NBI energy by approximately a factor 1.5. This acceleration was observed in a narrow pitch region, implying a velocity-space dependent mechanism, typical of wave-particle interaction phenomena, which are yet to be identified. The FI acceleration has also been decorrelated from the ELM crash, contrary to previous studies and in line with recent AUG observations.

# 5. CORE AND PEDESTAL PHYSICS

Plasma core and edge studies greatly benefited from improvements in diagnostic and modelling capabilities [46, 47, 48, 49, 50, 51, 52]. The capability of TCV's short-pulse reflectometry (SPR) system to measure turbulence amplitudes in the plasma outer-core region has been validated using a new synthetic diagnostic, based on local gyrokinetic GENE simulations coupled with the full-wave CUWA code [47]. These SPR capabilities made it possible to confirm reduced relative density-fluctuation levels in NT compared with PT plasmas, while revealing similar radial correlation lengths. With the help of Machine Learning methods, the applicability regime of the SPR could be extended to higher turbulence amplitudes than those accessible by traditional reflectometry methods [53]. Together with major hardware upgrades [48], the SPR system now further delivers 20-point edge density profiles every 400 ns, and allows for detailed studies of fast transient phenomena such as edge-localized modes. Further insights into plasma edge/pedestal physics were enabled by a new Doppler backscattering (DBS) system, installed to probe edge poloidal velocities  $(v_\perp)$ , radial electric field  $(E_r)$  profiles, and associated fluctuations in the upper low-field side region of the plasma [49]. Co-current NBI was found to consistently increase  $v_\perp$  in both limited and diverted configurations, in qualitative agreement with the expected response to toroidal torque, while

ECRH had only a modest effect. In diverted plasmas, the  $v_{\perp}$  profile and the related  $E_r$  well showed moderate variation with density and NBI, and no variation with changing helicity. Interestingly, however, the velocity shear kept increasing with increasing NBI power at the inner side of the  $E_r$  well, emphasizing the inner-well shear's role in the L-H transition.

In terms of edge/pedestal fluctuation studies, the first gyrokinetic GENE simulations of the TCV pedestal were carried out in the pre-ELM phase of 170kA, 1.1 MW NBI H-mode plasmas at two different levels of gas puffing, aimed at determining the role of electron temperature gradient (ETG) modes in pedestal transport [54]. These local, electron scale simulations showed that at low gas puffing, electron heat fluxes due to ETGs are negligible compared to the total experimental electron heat flux. At high gas puffing, instead, ETG-driven electron heat fluxes matched experimental values, suggesting that ETG modes become the limiting factor for pedestal formation. These simulations also highlighted the importance of toroidal-ETG, rather than slab-ETG, in these high gas puffing conditions.

Experimentally, inter-ELM edge fluctuations have been investigated with the Thermal Helium Beam (THB) diagnostic [51, 52], across a relatively large dataset of NBI and ECRH heated Type-I ELMy H-modes [55]. These discharges featured low gas puffing, plasma currents of 160 kA and 240 kA, and differ primarily in the amount of injected ECRH power. Coherent, inter-ELM fluctuations were identified around the separatrix, in the range of 30-90kHz. They appeared a few hundred microseconds after the ELM and showed a continuous frequency decrease before disappearing 0.3–0.5 ms prior to the next ELM crash. These fluctuations were primarily visible in electron density, without a clear signature in electron temperature. The frequency decrease correlated with a steepening of the pedestal density profile during the ELM cycle and, across discharges, showed a positive correlation with the injected heating power. Edge fluctuations were also investigated in the I-phase, an H-mode confinement regime characterized by so-called limit cycle oscillations (LCOs) or bursts that periodically flatten the plasma edge profiles [56]. Beyond its intrinsic interest, the I-phase is significant because of the proposed connection between LCOs and Type-III ELMs. Using Gas Puff Imaging (GPI), the I-phase was identified unambiguously on TCV for the first time and its distinction from L- and H-mode dithers was clearly demonstrated. A high-frequency edge mode (100–200 kHz) was observed as a precursor to the LCOs and the associated profile flattening, together with the resulting bursty two-dimensional filamentary transport in the SOL, was detailed.

Significant progress was also achieved in the study of electron cyclotron (EC) wave propagation and related diagnostic methods. Radiometer measurements on TCV [57] showed that Two-Plasmon Decay Instabilities (TPDIs) occur regularly in the TCV edge during X2 microwave injection in both L- and H-mode. These TPDIs are a class of parametric instabilities, where the gyrotron beam decays non-linearly into two upper hybrid waves with approximately half of the original frequency. They are caused by wave trapping in edge density fluctuations created by blobs or ELMs, and result in subsequent decays which correlate with fast ion generation and indicate Bernstein wave generation. Together with the work in [58], these findings clearly highlighted the importance of non-linear microwave propagation effects in view of ITER and DEMO, and could potentially be used on ECRH devices as a diagnostic for density fluctuations in the plasma edge or for concave density fluctuations in the confined plasma, e.g. due to rotating islands [59].

# 6. SOL AND DIVERTOR PHYSICS

SOL/divertor and exhaust studies advanced substantially on TCV, supported by improved diagnostic techniques, advanced modelling, and systematic experimental studies - with the removable divertor baffles remaining a central element.

Long outer divertor leg scenarios were extensively used to maximise diagnostic coverage of the divertor. Detailed measurements from existing diagnostics, including 2D maps of  $T_e$  and  $n_e$  from Divertor Thomson Scattering (DTS) achieved via outer leg sweeping, were complemented with new measurement capabilities of the Divertor Spectroscopy System (DSS) [60], the novel Toroidal DSS (TDSS) [61], and improved neutral pressure measurement capabilities [62]. Divertor  $T_i$  profiles were inferred with the DSS from Doppler broadening of C II, C III, and He II emission lines, in conditions ranging from strongly attached towards detached conditions [60]. These line-of-sight-integrated and emission-weighted measurements were compared to corresponding emission-weighted DTS electron temperature data and interpreted with a model for the divertor  $T_i$  evolution. This model predicts that the  $C^{2+}$  and  $He^+$  ion temperatures closely follow the main-ion temperature and reproduces the relative differences and agreements between measured ion temperatures and  $T_e$  in different divertor locations and regimes. While collisional coupling between the different species was found to be important in the divertor, upstream  $T_i$  and  $T_e$  measurements from CXRS and TS showed that ion and electron coupling plays a minor role in the edge plasma [63]. Instead, the upstream  $T_i/T_e$  ratio was found to mainly depend on the relative ion and electron heat fluxes from the core.

The above, as well as related studies, combined with progress in divertor transport code simulations, helped to

elucidate various aspects of divertor physics and to validate the numerical tools, SOLPS-ITER simulations of the TCV divertor and comparison with experiments identified a strong underprediction of molecular-related processes. This discrepancy was largely reconciled by using corrected molecular charge-exchange rates [64]. Molecular divertor spectroscopy further identified a significant increase of the rotational D<sub>2</sub> temperature during detachment and associated further divertor power and momentum losses, highlighting the impact of ion-molecule collisions [65]. Combining dedicated experiments and SOLPS-ITER simulations of TCV L-mode plasmas demonstrated synergistic benefits of impurity seeding and divertor baffling [66]. With baffles, divertor deuterium neutral density and compression increased. This increase was attributed to reduced neutral conductance between the divertor and main chamber, as quantified with a schematic neutral transport model. For a given seeding rate, baffling also strongly enhanced the divertor compression of neutral nitrogen. In contrast, the compression increase of nitrogen ions was less clear, and depended on changes in main-ion flows and ion temperature induced by baffling and seeding. SOLPS-ITER simulations were further challenged through validation against extensive experimental datasets. The near-sheath-limited, diverted L-mode reference case TCV-X21, originally developed for validating boundary turbulence codes, served as a benchmark. In a proof-of-principle approach, key input parameters (fuelling rate, particle diffusivity, and heat diffusivity) were optimised using a quantitative experiment-simulation agreement metric, and the resulting outputs were then compared with experimental measurements [67]. SOLPS-ITER validation efforts have also focused on dissipative divertor scenarios, with and without divertor baffles [68]. Earlier simulations predicted overly dense and cold divertor target conditions. Subsequent improvements, most notably in the treatment of ion flux limiters, led to significantly better agreement with experiment. Additional progress in core-edge coupling was obtained by including a convective transport contribution, motivated by JINTRAC.

The investigation of alternative divertor configurations (ADCs) [69] has continued to be a central theme on TCV, offering a promising route to optimize exhaust handling in DEMO and likely constituting a necessity for the high-field, compact fusion approach. The individual roles of key geometric divertor parameters in power exhaust have been thoroughly revisited, supported by enhanced diagnostic capabilities, improved theoretical understanding, and the recent ability to routinely obtain SOLPS-ITER simulations of TCV plasmas - including drifts - with orders-of-magnitude improvement in convergence speed [70].

In systematic L-mode density scans, the impact of poloidal and total flux expansion, the key features of the X-Divertor (XD) and the Super-X Divertor (SXD), on the detachment threshold were shown to be smaller than expected from simple analytical models [71]. Substantially larger improvements were obtained from extending the outer divertor leg length. These results compare favourably with SOLPS-ITER simulations and elucidated the role of plasma drifts, parallel flows, and power and momentum losses in reproducing the experiments - effects that are typically neglected or only partially included in analytical models.

Strong power exhaust benefits were demonstrated in the X-Point Target (XPT) divertor geometry, which incorporates a secondary X-point located near the divertor target. Experiments on TCV revealed a novel X-point radiator regime, the X-point target radiator (XPTR), that forms at this secondary X-point [72], Fig. 4. Unlike the conventional X-point radiator regime discussed in Sec. 2, the XPTR spatially decouples the radiator from the confined plasma, thereby preventing unwanted radiative cooling of the edge. This separation offers promising prospects for coreedge integration, as it mitigates proximity to operational limits and helps preserve core performance. In the Ohmic XPT plasmas studies in [72], detachment was accessed far more readily than in standard single-null (SN) configurations, with divertor target heat fluxes reduced by more than a factor of five. This

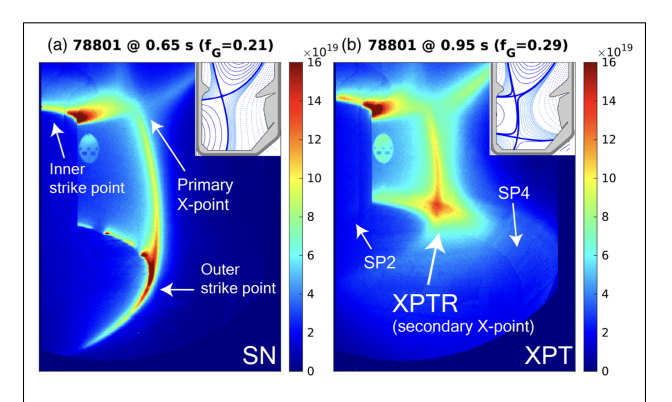


FIG. 4.  $D_{\alpha}$  filtered images showing the XPTR development during the transition from (a) SN to (b) XPT. Insets show the magnetic equilibria. Fig. from [72].

was accompanied by the emergence of a stable, localised radiative zone around the secondary X-point, whose position showed remarkable insensitivity to upstream density variations - an increase in robustness exceeding a factor of five compared to the SN case. Enhanced detachment front position resilience against fueling, seeding, and heating perturbations was further demonstrated at dynamic timescales, which is key in view of facilitating real-time detachment control [73]. Extended to Type-I ELMy H-mode, XPT operation also showed strong indications of passive mitigation of large transient heat loads caused by ELMs [74], which could substantially increase the maximum allowed ELM size in future reactors.

The relative importance of divertor and outboard midplane fluctuation-induced radial particle fluxes has been in-

vestigated with fast reciprocating probe measurements in L-mode discharges of varying collisionality and divertor geometry [75]. Both at low and high collisionality, within one power fall-off length of the separatrix, the radial particle flux in the divertor was found to be small - only about 20% of that at the outboard midplane. Fluctuation characteristics were found to be consistent with a resistive X-point turbulence regime, with a possible transition to a resistive ballooning regime at high density. Interestingly, in the inter-null region of the snowflake divertor, where increased cross-field transport is often predicted, a reduction of up to 50% compared to the single-null geometry was observed. A follow-up study [76] specifically investigated conditions at detachment onset. Results showed that upstream density profile broadening in these conditions was associated with a 2- to 4-fold increase in the fluctuation-induced radial particle flux in the vicinity of the X-point and further upstream. In contrast, radial transport downstream of the dissipative region remained at levels similar to those in attached conditions.

# 7. CONTROL

Improvements in plasma control, through model-based and data-driven methods, have been a growing focus of recent TCV activities. TCV's flexible, digital, distributed control system underwent major hardware and software upgrades and, after years of development, evolved from an experimental setup into a stable and reliable platform [77]. This system, called SCD (in French Système de Contrôle Distribué), is based on three pillars: MATLAB Simulink, the MARTe2 real-time control framework, and MDSplus. The SCD controls, in real time, TCV's 19 independent coil power supplies, 13 gas injection valves, multiple steerable EC launchers, and two NBIs and several gyrotrons with continuously adjustable power. Most legacy real-time codes, such as magnetic reconstructions, MHD mode analysis, the RAPTOR transport simulator and the RAPDENS electron density observer, have already been ported to the new framework. Increasingly, the SCD also integrates real-time capable diagnostics, a trend further strengthened by the recent inclusion of the Data Distribution Service (DDS) [78]. These diagnostics currently include 117 Thomson Scattering lines of sight, 10 filtered camera images (MANTIS), 14 far-infrared interferometry chords (FIR), 64 fast magnetic probes, and 120 bolometry lines of sight (Radcam).

The SCD combines sufficient flexibility to allow rapid prototyping and implementation of new ideas with the necessary rigor to ensure long-term algorithm maintenance. Over the past two years, it has been at the heart of numerous advances in tokamak control. These include, but are not limited to, the following: A model-based plasma breakdown design combined with a shot-to-shot correction algorithm based on Iterative Learning Control (ILC) to accelerate the development of robust plasma start-up [79]; Real-time estimates of the vertical instability growth rate refined by incorporating the effects of radial displacements [80], to enhance vertical plasma control; Development of an alternative data-driven approach for vertical control, including the recent adaptation of the Extremum Seeking-based Vertical Stabilisation control algorithm [81]; Design, implementation, and experimental validation of a novel, real-time, model-based shape controller [82], using an isoflex approach with improved interpretability developed in [83]; Further development of TCV's alternative magnetic control approach based on Reinforcement Learning (RL) [84]; Experimental testing of the Current Limit Avoidance (CLA) system foreseen for PF coil current saturation avoidance in ITER [85]; Improved estimation of the dynamic evolution of the electron density profile using RAPDENS with an Extended Kalman Filter (EKF), constrained by low-frequency Thomson scattering measurements and high-frequency, line-integrated interferometry measurements [86]; Automatic, real-time labelling of confinement states through data-driven models incorporating uncertainty quantification and robustness [87]; Development of an interpretable representation of the plasma operational space with respect to disruption limits, projecting plasma behaviour as continuous trajectories in a low-dimensional latent space and estimating proximity to disruptions [88]; Demonstration of divertor emission front/detachment control during strike-point sweeping [89]; Extensive multi-device investigation of exhaust dynamics in response to deuterium fuelling, impurity seeding, and plasma heating, providing benchmarks for the validation of dynamical, physics-based heat exhaust and SOL models for model-based designs of detachment controllers.

# 8. OUTLOOK

Moving forward, TCV will continue to investigate key physics questions in support of ITER and to further develop concepts and operational regimes aimed at optimizing the tokamak concept for future fusion power plants, leveraging its strong operational flexibility and versatility. Synergies will be further strengthened across the EU-ROfusion devices and with partners beyond, including both public and private initiatives. In the near term, two additional 1 MW dual-frequency gyrotrons will be installed, significantly increasing the available ECRH power. Another upgrade in progress is the installation of a passive in-vessel helical coil, the Runaway Electron Mitigation Coil (REMC), designed to address the challenge of post-disruption runaway-electron beams. During a current quench, the induced currents in the REMC are expected to generate 3D magnetic perturbations that break up

nested flux surfaces and suppress RE beam formation [90]. A further major upgrade underway is the testing of the Tightly-Baffled, Long-Legged Divertor (TBLLD)[91], a novel exhaust concept that combines an extended divertor leg with a strong poloidal neutral pressure gradient achieved via tight baffling. This configuration is predicted to enhance power exhaust capabilities by up to a factor of five, while minimizing additional engineering complexity, making it attractive for reactor-scale implementation. Finally, TCV and, more broadly, SPC will continue to place high priority on the education and training of the next generation of fusion scientists and engineers. In parallel, TCV will also pursue more exploratory topics, such as the properties and performance of the Doublet configuration, which was stabilized successfully for the first time only a few weeks ago - overcoming a decades-long challenge and opening the door to a new line of investigation.

# **ACKNOWLEDGEMENTS**

This work has been carried out within the framework of the EUROfusion Consortium, partially funded by the European Union via the Euratom Research and Training Programme (Grant Agreement No 101052200 — EU-ROfusion). The Swiss contribution to this work has been funded by the Swiss State Secretariat for Education, Research and Innovation (SERI). Views and opinions expressed are however those of the author(s) only and do not necessarily reflect those of the European Union, the European Commission or SERI. Neither the European Union nor the European Commission nor SERI can be held responsible for them. This work was supported in part by the Swiss National Science Foundation.

# REFERENCES

- [1] HOFMANN, F., LISTER, J. B., ANTON, W., et al., Plasma Phys. Controlled Fusion, 36 12B (1994) B277.
- [2] DUVAL, B., ABDOLMALEKI, A., AGOSTINI, M., et al., Nucl. Fusion, 64 11 (2024) 112023.
- [3] JOFFRIN, E., WISCHMEIER, M., BARUZZO, M., et al., Nucl. Fusion, 64 11 (2024) 112019.
- [4] KARPUSHOV, A. N. et al., Fusion Engineering and Design, 187 (2023) 113384.
- [5] SIRAVO, U., DUBRAY, J., ELAIAN, H., et al., Fusion Engineering and Design, 201 (2024) 114277.
- [6] MOLINA-CABRERA, P., PASTORE, F., FRANK, A., et al. (2025). in preparation.
- [7] LABIT, B., SAUTER, O., PÜTTERICH, T., et al., Plasma Phys. Controlled Fusion, 66 2 (2024) 025016.
- [8] FRASSINETTI, L. et al., preprint, 30th IAEA Fusion Energy Conference, Chengdu, China (2025).
- [9] LABIT, B., BAGNATO, P., DUVAL, B. P., et al., Plasma Phys. Controlled Fusion, 67 5 (2025) 055010.
- [10] CODA, S. et al., preprint, 30th IAEA Fusion Energy Conference, Chengdu, China (2025).
- [11] DUNNE, M. et al., preprint, 30th IAEA Fusion Energy Conference, Chengdu, China (2025).
- [12] LABIT, B. et al., 51th European Physical Society Conference on Plasma Physics (2025).
- [13] STAGNI, A., VIANELLO, N., AGOSTINI, M., et al., Nucl. Fusion, 64 2 (2024) 026016.
- [14] BERNERT, M., BOSMAN, T., LUNT, T., et al., Nucl. Mater. Energy, 43 (2025) 101916.
- [15] SUN, G., PAN, O., BERNERT, M., et al., arXiv preprint arXiv:2311.07295 (2025).
- [16] REIMERDES, H., THEILER, C., BERNERT, M., et al., Nucl. Mater. Energy, 41 (2024) 101784.
- [17] FÉVRIER, O. et al., preprint, 30th IAEA Fusion Energy Conference, Chengdu, China (2025).
- [18] FÉVRIER, O. et al., *Plasma Phys. Controlled Fusion*, **66** 6 (2024) 065005.
- [19] TONELLO, E., MOMBELLI, F., FÉVRIER, O., et al., Plasma Phys. Controlled Fusion, 66 6 (2024) 065006.
- [20] DURR-LEGOUPIL-NICOUD, G., FÉVRIER, O., THEILER, C., et al. (2025). in preparation.
- [21] LIM, K., GIACOMIN, M., RICCI, P., et al., Plasma Phys. Controlled Fusion, 65 8 (2023) 085006.
- [22] MORGAN, R. I., DURR-LEGOUPIL-NICOUD, G. H. S., FÉVRIER, O., et al., Nucl. Fusion (2025).
- [23] MOMBELLI, F., MASTROGIROLAMO, A., TONELLO, E., et al., arXiv preprint arXiv:2506.03966 (2025).
- [24] MUSCENTE, P., INNOCENTE, P., BALL, J., et al., Nucl. Mater. Energy, 34 (2023) 101386.
- [25] DURR-LEGOUPIL-NICOUD, G. et al., 51th European Physical Society Conference on Plasma Physics (2025).
- [26] BALESTRI, A., BALL, J., CODA, S., et al., Plasma Phys. Controlled Fusion, 66 7 (2024) 075012.
- [27] BALESTRI, A. et al., 51th European Physical Society Conference on Plasma Physics (2025).
- [28] DI GIANNATALE, G., BOTTINO, A., BRUNNER, S., et al., Plasma Phys. Controlled Fusion, 66 9 (2024) 095003.
- [29] BALESTRI, A., MANTICA, P., MARIANI, A., et al., Plasma Phys. Controlled Fusion, 66 6 (2024) 065031.
- [30] MARIANI, A., AUCONE, L., BALESTRI, A., et al., Nucl. Fusion, 64 10 (2024) 106024.
- [31] DECKER, J., HOPPE, M., SHEIKH, U., et al., Nucl. Fusion, 64 10 (2024) 106027.
- [32] WIJKAMP, T., HOPPE, M., DECKER, J., et al., Nucl. Fusion, 64 1 (2023) 016021.
- [33] SHEIKH, U. et al., preprint, 30th IAEA Fusion Energy Conference, Chengdu, China (2025).
- [34] TONELLO, E. et al., Joint Runaway Electron Modelling (REM) and WPTE RT03 Analysis meeting, Lausanne (2025).
- [35] HOPPE, M., DECKER, J., SHEIKH, U., et al. (2025). in preparation.
- [36] SIMONS, L., CEROVSKY, J., DECKER, J., et al., Rev. Sci. Instrum. 96 9 (2025) 093501.

- [37] POLEY-SANJUÁN, J., SIMONS, L., VUUREN, A. J. V., et al. (2025). in preparation.
- [38] POLEY-SANJUÁN, J., CLÉMENT, A., FASOLI, A., et al., Nucl. Fusion, 65 7 (2025) 076006.
- [39] POLEY-SANJUÁN, J., CLÉMENT, A., FASOLI, A., et al., Rev. Sci. Instrum. 96 8 (2025) 083504.
- [40] SCHMIDT, B. S., POLEY-SANJUÁN, J., et al., Plasma Phys. Controlled Fusion, 66 4 (2024) 045004.
- [41] MAZZI, S., VALLAR, M., KUMAR, U., et al., Frontiers in Physics, 11 (2023) 1225787.
- [42] DREVAL, M., SHARAPOV, S., JANSEN VAN VUUREN, A., et al., Nucl. Fusion, 65 1 (2024) 016037.
- [43] VUUREN, A. V. et al., preprint, 30th IAEA Fusion Energy Conference, Chengdu, China (2025).
- [44] POLEY-SANJUÁN, J., JANSEN VAN VUUREN, A., et al., Nucl. Fusion, 65 9 (2025) 092006.
- [45] POLEY-SANJUÁN, J., VUUREN, A. J. V., GALDÓN-QUIROGA, J., et al. (2025). in preparation.
- [46] HAMM, D., THEILER, C., SIMEONI, M., et al. (2025). in preparation.
- [47] KRUTKIN, O., KUMAR, U., MAZZI, S., et al., Nucl. Fusion, 64 2 (2024) 026010.
- [48] KUMAR, U., CODA, S., ROSSEM, M. V., et al. (2025). in preparation.
- [49] RIENÄCKER, S., HENNEQUIN, P., VERMARE, L., et al., Plasma Phys. Controlled Fusion, 67 6 (2025) 065003.
- [50] RIENÄCKER, S., HENNEQUIN, P., VERMARE, L., et al. (2025). in preparation.
- [51] UGOLETTI, M., AGOSTINI, M., LA MATINA, M., et al., Rev. Sci. Instrum. 95 8 (2024) 083530.
- [52] AGOSTINI, M., MATINA, M. L., UGOLETTI, M., et al. (2025). in preparation.
- [53] KRUTKIN, O., BRUNNER, S., CODA, S., et al., Plasma Phys. Controlled Fusion, 67 5 (2025) 055040.
- [54] KRUTKIN, O., CHAPMAN-OPLOPOIOU, B., et al., Plasma Phys. Controlled Fusion, 67 2 (2025) 025029.
- [55] LA MATINA, M., AGOSTINI, M., UGOLETTI, M., et al., Plasma Phys. Controlled Fusion, 67 8 (2025) 085034.
- [56] GRIENER, M., WÜTHRICH, C., WANG, Y., et al., Nucl. Fusion, 65 1 (2024) 016041.
- [57] CLOD, A., SENSTIUS, M. G., NIELSEN, A. H., et al., Phys. Rev. Lett. 132 (2024) 135101.
- [58] CAZABONNE, J., CODA, S., DECKER, J., et al., Nucl. Fusion, 64 2 (2024) 026019.
- [59] CLOD, A., RAGONA, R., SENSTIUS, M. G., et al., Plasma Phys. Controlled Fusion, 66 12 (2024) 125001.
- [60] MARTINELLI, L., MIKITCHUK, D., DUVAL, B., et al., Nucl. Fusion, 65 5 (2025) 056017.
- [61] DUCKER, R., MYKYTCHUK, D., DUVAL, B. P., et al. (2025). in preparation.
- [62] SUN, G., REIMERDES, H., ELAIAN, H., et al. (2025). in preparation.
- [63] CAVEDON, M., BRIDA, D., BAGNATO, F., et al. (2025). in preparation.
- [64] VERHAEGH, K., WILLIAMS, A., MOULTON, D., et al., Nucl. Fusion, 63 7 (2023) 076015.
- [65] OSBORNE, N., VERHAEGH, K., MOULTON, D., et al. (2025). in preparation.
- [66] SUN, G., REIMERDES, H., THEILER, C., et al., Nucl. Fusion, 65 2 (2025) 026061.
- [67] WANG, Y., COLANDREA, C., OLIVEIRA, D., et al., Nucl. Fusion, 64 5 (2024) 056040.
- [68] TONELLO, E. et al., preprint, 30th IAEA Fusion Energy Conference, Chengdu, China (2025).
- [69] VERHAEGH, K. et al., preprint, 30th IAEA Fusion Energy Conference, Chengdu, China (2025).
- [70] CARPITA, M., TONELLO, E., COLANDREA, C., et al. (2025). in preparation.
- [71] CARPITA, M. et al., 9th Asia-Pacific Conference on Plasma Physics, Fukuoka (2025).
- [72] LEE, K., THEILER, C., CARPITA, M., et al., Phys. Rev. Lett. 134 (2025) 185102.
- [73] WINKEL, M. et al. (2025). in preparation.
- [74] ZURITA, M. et al., 67th Annual Meeting of the APS Division of Plasma Physics (DPP), Long Beach, California (2025).
- [75] TSUI, C. K., BOEDO, J. A., MYRA, J. R., et al., Physics of Plasmas, 31 2 (2024) 022506.
- [76] RIZKALLAH, R., BOEDO, J. A., TSUI, C. K., et al. (2025). in preparation.
- [77] GALPERTI, C., FELICI, F., VU, T., et al., Fusion Engineering and Design, 208 (2024) 114640.
- [78] MASOCCO, R., TENAGLIA, A., GALPERTI, C., et al., Fusion Engineering and Design, 221 (2025) 115344.
- [79] GRAZIA, L. E. di, FELICI, F., MATTEI, M., et al., Nucl. Fusion, 64 9 (2024) 096032.
- [80] MARCHIONI, S., FELICI, F., SAUTER, O., et al. (2025). in preparation.
- [81] DUBBIOSO, S., DE TOMMASI, G., GALPERTI, C., et al., Fusion Engineering and Design, 219 (2025) 115198.
- [82] MELE, A., TENAGLIA, A., FELICI, F., et al. (2025). in preparation.
- [83] TENAGLIA, A., PESAMOSCA, F., FELICI, F., et al., Fusion Engineering and Design, 207 (2024) 114618.
- [84] TRACEY, B. D., MICHI, A., CHERVONYI, Y., et al., Fusion Engineering and Design, 200 (2024) 114161.
- [85] FRATTOLILLO, D., MELE, A., GALPERTI, C., et al., 67 5 (2025) 055017.
- [86] PASTORE, F., FELICI, F., BOSMAN, T., et al., Fusion Engineering and Design, 192 (2023) 113615.
- [87] POELS, Y., VENTURINI, C., PAU, A., et al. (2025). in preparation.
- [88] POELS, Y., PAU, A., DONNER, C., et al. (2025). in preparation.
- [89] BOSMAN, T. O. S. J., KOENDERS, J. T. W., PEREK, A., et al. (2025). in preparation.
- [90] BATTEY, A. et al. (2025). in preparation.
- [91] REIMERDES, H. et al., preprint, 30th IAEA Fusion Energy Conference, Chengdu, China (2025).